International Journal Of
Industrial Electronics Control and Optimization
Print ISSN: 3517-2645
Online ISSN: 3568-2645
Homepage: https://ieco.usb.ac.ir/

Controlling and Estimating the Speed of Shaking Table by Fusing Camera, Encoder and Accelerometer using AUKF and Fuzzy Sliding Mode Controller

Nima Rajabi Namini[1] | Ramazan Havangi[2] , Amir Hossein Abolmasoumi[3]
Faculty of Electrical Engineering and Computer, University of Birjand, Iran.[1,2]
Electrical Engineering department, Arak University, Arak, Iran Iran.[3]
Corresponding author's email: Havangi@Birjand.ac.ir

Article Info

Article type:
Research Article

Article history:
Received: **********
Received in revised form: **********
Accepted: **********
Published online: **********

Keywords:
Earthquake Simulator,
Multi-Sensor Data Fusion,
Fuzzy,
Sliding Mode Control

ABSTRACT

An earthquake is a sudden and destructive natural disaster that often results in unpredictable damage to human life and property. Investigating the effects of earthquakes on buildings and enhancing the seismic performance of structures is a crucial approach to mitigating severe damage during such events. One effective tool in testing the resistance of structures against earthquakes is the use of shaking tables. In this paper, the stabilization and control of an earthquake simulator using a fuzzy sliding mode controller (FSMC), an adaptive unscented Kalman filter (AUKF), and an adaptive extended Kalman filter (AEKF) are presented. These filters employ a recursive technique to effectively adjust the noise covariance by utilizing an adaptation method known as the steepest descent. In the proposed approach, the shaking table states are estimated using an accelerometer, encoder, and camera. These estimated states are then utilized by the AEKF/AUKF to stabilize and control the closed-loop system. A fuzzy sliding mode controller is designed to track the reference input and eliminate external disturbances and noise. In sliding mode control, the occurrence of chattering in the control input is unavoidable. To mitigate this undesired chattering phenomenon, a fuzzy inference mechanism has been employed. The image processing approach has been utilized to measure the displacement online using the camera. The advantages of using the camera include not requiring direct contact with the table, as well as offering a low cost and good accuracy. The performance of the proposed method has been examined using the shaking table at the Research Center of Arak University. The obtained results indicate that the suggested method exhibits a high level of efficiency.

NOMENCLATURE

F	Linear force	β	Viscous damping coefficient
p	Number of pole pairs	T_e	Electromagnetic torque
i_d , i_q	Currents on the d and q axes	u_{eq}	Equivalent control input
v_d , v_q	Voltages on the d and q axes	u_{sw}	Switching control input
T	Torque of motor	T_l	Load torque
L_d,L_q	Inductances on d- and q-axes	λ	Flux amplitude
R	Motor winding resistance	η	Ball-screw efficiency
Ω	Angular velocity of the rotor	h	Lead of the ball screw
Θ	Angular displacement of the motor shaft	M	Total mass of the stage
J	Moment of inertia	φ	Boundary layer thickness in FSMC
ξ	Ball-screw efficiency	s	Sliding surface variable
$\tilde{x}$	Tracking error	$\dot{\omega}_{des}$	Desired acceleration signal
		I	Image matrix

I. Introduction

Seismic shake tables serve as indispensable tools for studying the dynamic response of structures subjected to earthquake-like excitations [1–2]. Depending on the application scale and power requirements, these systems typically employ hydraulic or electric actuation[3-4]. Hydraulic mechanisms, characterized by high power density and large stroke capability, are favored for large-scale shaking tables, while electric actuation is generally restricted to smaller laboratory setups [5-6].

Despite substantial advancements in actuation technology and control system design, accurately reproducing complex seismic excitations, particularly acceleration profiles, remains a formidable challenge [7–9]. Small displacement tracking errors can magnify through differentiation, leading to significant inaccuracies in acceleration reproduction. Furthermore, factors such as mechanical backlash, environmental disturbances, system nonlinearities, and sensor imperfections exacerbate this difficulty [10-12].

Previous studies have attempted to improve shaking table performance through various control strategies, including feedforward compensation [13], iterative learning control (ILC) [14], and adaptive control techniques such as minimal control synthesis and model reference adaptive control [15–18]. Additionally, robust controllers like sliding mode control (SMC) have been explored to address system uncertainties and disturbances [19–20]. Despite the success of these methods, they often face limitations: conventional Kalman filtering approaches assume fixed noise statistics, making them vulnerable to model mismatches and variations in measurement noise. While SMC approaches offer robustness, they suffer from undesirable chattering phenomena, which can compromise actuator lifespan and energy efficiency [21-23]. Furthermore, traditional sensor setups that rely heavily on encoders are prone to mechanical degradation, high costs, and installation complexity. Thus, a critical research gap exists: the lack of an integrated approach that simultaneously addresses sensor noise, dynamic system uncertainties, and controller chattering in a practical, cost-effective manner. This study proposes a novel solution by combining adaptive sensor fusion techniques with an intelligent robust control strategy to achieve superior tracking performance [24-26].

In recent years, artificial intelligence (AI)-based control strategies—such as fuzzy logic, neural networks, and adaptive neuro-fuzzy inference systems have attracted considerable interest in the field of seismic control of shaking tables due to their ability to manage nonlinear dynamics and model uncertainties effectively [27, 28]. These methods provide adaptive learning mechanisms that can enhance robustness and suppress undesirable chattering phenomena typically observed in classical sliding mode controllers [29]. Despite these advantages, AI-based control approaches are not without limitations. They often require large datasets for training, exhibit sensitivity to sensor noise, and can encounter challenges in real-time applications due to their computational demands. Moreover, their performance is highly dependent on appropriate design choices, such as the tuning of membership functions in fuzzy systems or the architecture of neural networks. Additionally, unlike conventional model-based techniques, providing formal stability guarantees for AI-based controllers remains an ongoing challenge [30]. Recent advancements, particularly in deep learning, have further expanded the potential of AI in control applications. Methods such as deep reinforcement learning and neural adaptive controllers have demonstrated superior performance in managing highly nonlinear and time-varying systems, particularly in high-uncertainty environments [31–33]. Nevertheless, the application of these advanced techniques to shake table control is still in its early stages and presents a promising direction for future research [34].

Motivated by the aforementioned challenges, This paper presents the design and implementation of a fuzzy sliding mode controller integrated with adaptive estimation filters—namely the AEKF and AUKF—for a laboratory-scale seismic shake table system. The primary objective is to develop an efficient control strategy capable of accurately tracking scaled earthquake excitations, even in the presence of parameter uncertainties and unmodeled dynamics. Particular emphasis is placed on acceleration tracking performance throughout the study. The proposed control framework integrates measurements from encoder sensors, a vision-based camera system, and an accelerometer using the AEKF/AUKF to estimate the system states. These estimated states are then used within the FSMC to ensure precise trajectory tracking. The authors believe that the full integration of the AEKF/AUKF measurement fusion filter and FSMC, along with the corresponding hardware and software implementation, constitutes an innovative and cost-effective solution. This framework holds significant potential for future deployment in commercial shake tables used in earthquake engineering applications.
The main contributions of this paper are summarized as follows:

Adaptive Sensor Fusion: Development of a multi-sensor fusion system combining MEMS accelerometers, encoders, and vision-based displacement measurements, with online adaptation of Kalman filter noise covariances for improved state estimation under nonlinear and noisy conditions.

Chattering-Reduced Robust Control: Design of a fuzzy sliding mode control strategy that dynamically regulates the switching surface boundary, reducing chattering effects without compromising robustness.

Practical Implementation: Realization and experimental validation of the proposed approach on a power screw-driven

seismic simulator, demonstrating superior tracking accuracy, disturbance rejection, and robustness compared to conventional control techniques.

The remainder of the paper is organized as follows: Section 2 describes the system modeling and problem formulation. Section 3 presents the sensor fusion design using adaptive Kalman filters. Section 4 details the proposed fuzzy sliding mode controller. Section 5 discusses experimental validation and performance analysis. Finally, Section 6 concludes the paper and outlines directions for future research.

II. Dynamic Model of the System

To derive the system dynamics and facilitate the subsequent control design, the following assumptions are adopted. Sensor noise and drift are bounded and mitigated using adaptive Kalman filtering. Actuator dynamics are considered sufficiently fast relative to the system dynamics, allowing actuator lag to be neglected. External disturbances and modeling uncertainties are assumed to be bounded and modeled as additive terms. The shake table operates within its linear elastic range, and the initial system states are assumed to be measurable or reasonably estimable through multi-sensor fusion. These assumptions are standard and ensure the robustness and practical applicability of the proposed method. The d and q coordinate systems serve as mathematical converters for analysing and modelling three-phase circuits[27].

$$\begin{aligned}\frac{di_d}{dt} &= \frac{v_d}{L_d} - \frac{Ri_d}{L_d} + \frac{L_q}{L_d} p\omega i_q \\ \frac{di_q}{dt} &= \frac{v_q}{L_q} - \frac{Ri_q}{L_q} + \frac{L_d}{L_q} p\omega i_d - \frac{\lambda p\omega}{L_d} \\ T_e &= \frac{3}{2}((L_d - L_q) i_q i_d + \lambda i_q) p\end{aligned} \quad (1)$$

where i_d and i_q are the currents on the d and q axes, espectively. Similarly, for the inductances on these axes, we use the symbols L_d and L_q. The voltages on the d and q axes, we denote them as v_d and v_q respectively. The symbol ω represents the angular velocity of the rotor. λ Signifies the flux amplitude. Furthermore, we introduce two more variables: p denotes the number of pole pairs, while T_e represents the electromagnetic torque. The dynamic equations that describe the motion of a motor shaft can be stated as follows:

$$\frac{d}{dt}\omega = \frac{1}{J}\left(T_e - \beta\omega - T_l\right) \quad (2)$$

$$\frac{d\theta}{dt} = \omega \quad (3)$$

where β denotes the viscous damping coefficient associated with the motor bearings, θ is the angular displacement of the shaft, and T_l signifies the load torque acting on the motor shaft[3]. Then, the mechanism of the ball screw is also represented in the following manner.

$$T = \frac{FL}{\xi} \quad (4)$$

where T is the torque generated by the motor, F is linear force, ξ is ball-screw efficiency, and L stands for the lead of the ball screw. For a normal screw wing, the efficiency is approximately 90% [27]. Equation (5) establishes a relationship between the driving force and the rotational acceleration of the ball-screw. By substituting Equation (6) into Equation (2), the fundamental dynamic equation governing the motion of the electric motor shaft can be reformulated, resulting in Equation (7).

$$F = ML\ddot{\theta} \quad (5)$$

$$T_l = \frac{ML^2\ddot{\theta}}{\xi} \quad (6)$$

$$j\frac{d\omega}{dt} = T_e - \beta\omega - \frac{ML^2\ddot{\theta}}{\xi} \quad (7)$$

The term $\ddot{\theta}$ denotes the rotational acceleration of the motor shaft. Additionally, M signifies the combined mass of the stage. This relationship is expressed in (8),

$$M = m + m_1 \quad (8)$$

By rearranging equations (7) and (8):

$$\left(j + \frac{ML^2}{\xi}\right)\frac{d\omega}{dt} = T_e - \beta\omega \quad (9)$$

$$\frac{d\omega}{dt} = \frac{1}{J}\left(T_e - \beta\omega\right) \quad (10)$$

$$J = j + \frac{mL^2}{\xi} \quad (11)$$

FSMC for trajectory tracking of shake table with adaptive filtering

Figure 1 shows the schematic diagram of the PMSM/Shake Table system. Data fusion is essential for accurately estimating the system's displacement, velocity, and acceleration by integrating measurements from a MEMS accelerometer, encoder, and camera. Image processing provides advantages over traditional encoders and cameras in displacement measurement for shaking tables, such as non-contact operation, high spatial resolution, adaptability, robustness, and the ability to capture contextual information.

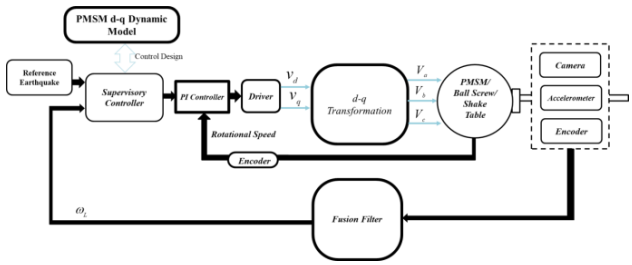

Fig.1. Communication diagram of components and supervisor controller

Accelerometers perform well at higher frequencies but lose accuracy at lower frequencies due to sensitivity to low-frequency noise and reduced signal resolution. These low-frequency errors can significantly impact the stability of closed-loop systems, as they are amplified when differentiated to calculate velocity and displacement. This leads to challenges in tracking low-frequency seismic components, causing potential instability or performance degradation.

To address these issues, adaptive filtering and multi-sensor fusion with systems like encoders and cameras are crucial for improving control system reliability and stability. The data fusion process in AEKF and AUKF follows a recursive procedure. Initially, sensor data—displacement from the encoder, acceleration from the accelerometer, and visual data from the camera—are inputs. In the prediction step, AEKF and AUKF algorithms forecast the next system state using a dynamic model. The update step incorporates actual sensor measurements to refine the predicted states.

In AEKF, the correction is based on a linearized model using Jacobian matrices to approximate the system's nonlinear dynamics. Conversely, AUKF uses the unscented transformation to directly propagate the mean and covariance through nonlinear functions, avoiding linearization. This enables AUKF to better handle nonlinearities in sensor data. Both AEKF and AUKF adaptively update noise covariance matrices, a critical feature given the variability in measurement noise caused by environmental conditions or sensor performance. A recursive adaptation rule adjusts the noise covariance matrices dynamically, ensuring filter robustness and enhancing state estimation accuracy over time.

A. Fuzzy-Sliding-Mode Supervisory Controller

Developing an effective controller to accurately follow the desired acceleration trajectory of a shake table involves numerous challenges, mainly due to system nonlinearities and environmental uncertainties. The presence of friction, actuator saturation, and nonlinear electrical or hydraulic dynamics complicates modeling and control design.

Remark 1 : Nonlinearities such as actuator saturation and friction introduce unpredictable behavior that cannot be fully captured by linear models, necessitating adaptive and robust control approaches like FSMC.

Moreover, acceleration, being the second derivative of displacement, amplifies any noise or error present in displacement or velocity measurements. Low-frequency noise and sensor limitations further degrade feedback quality, making precise trajectory tracking difficult. External disturbances such as temperature variations and varying payloads also affect system dynamics.

Remark 2. Errors in displacement or velocity are magnified in acceleration, particularly at low frequencies—making noise rejection and real-time adaptability essential for accurate tracking.

To overcome these challenges, this study integratesFSMC with AUKF. The combined scheme aims to achieve robust tracking of earthquake-like signals under two key uncertainties:

Model uncertainties, arising from unaccounted system dynamics.

Payload inconsistencies, caused by the installation of various structures on the shake table during experiments.

The shake table control system consists of two loops. The first loop uses a proportional-integral (PI) controller to track the control input. The second loop is a supervisory controller that monitors the overall system performance. Since the motor controller operates with a PI configuration, the supervisory FSMC ensures robust system behavior. By integrating AEKF/AUKF techniques into closed-loop velocity control, the system achieves precise control over velocity and acceleration.

The FSMC is specifically designed to regulate the shake table's velocity, with the sliding surface defined as detailed in [29]. This approach effectively handles dynamic system behavior and ensures accurate trajectory tracking, even under varying experimental conditions. The sliding surface s is selected based on the system's states, as defined below:

$$s(x,t)=\left(\frac{d}{dt}+\alpha\right)^{n-1}\tilde{x} \tag{12}$$

Here, $\tilde{x}$ is the tracking error between the reference trajectory and the actual state of the system, the parameter n represents the order of the governing dynamic equations, α denotes a constant that is strictly positive.The choice of the sliding surface (S) is determined by the system states, with $s(x,t)=\tilde{x}$ [30]. Employing equation (1), the time derivative for S is as:

$$\dot{s}(t)=\frac{1}{J}\left(T_e-\beta\omega-T_l\right)-\dot{\omega}_{des} \tag{13}$$

The desired acceleration signal, denoted as $\dot{\omega}_{des}$, is bounded, meaning there exists a positive constant L such that: $\left|\dot{\omega}_{des}(t)\right|\le L$, $\forall\, t\ge 0$.The control input is also defined as (14) where u_{eq} is the equivalent control and is obtained from (15).

$$u = u_{eq} - u_{reach} \tag{14}$$

To obtain the equivalent control law necessary for the electric torque here, we derive the following relationship by setting equation (13) equal to zero.

$$u_{eq} = \hat{\beta}\omega + T_l + \hat{J}\dot{\omega}_{des} \tag{15}$$

where $\hat{\beta}$, and $\hat{J}$ are estimated values of β, and J parameters, respectively. To ensure the stability of the sliding surface using the Lyapunov stability theory, we initially consider the selected Lyapunov function as follows:

$$V(s) = \frac{1}{2}S^2 \tag{16}$$

which is a positive definite function.

$$\dot{V}(s) = \frac{1d}{2dt}S^2 \le -\eta|S|, \eta \ge 0 \tag{17}$$

where η is a positive non-Fer constant, when inequality (17) is achieved, it indicates that the system is both stable and well-regulated. u_{reach} is also calculated as (18) satisfying the sliding condition.

$$u_{reach} = ksgn(S) \tag{18}$$

To achieve the intended sliding behaviour, it is necessary to select the controller output is as:

$$u = \hat{\beta}\omega + T_l + \hat{J}\dot{\omega}_{des} - ksgn(S) \tag{19}$$

To reduce the chattering caused by control command, we propose the implementation of a boundary layer with a thickness φ. Consequently, Equation (19) is reformulated as follows:

$$u = \hat{\beta}\omega + T_l + \hat{J}\dot{\omega}_{des} - ksat\left(\frac{s}{\varphi}\right) \tag{20}$$

The sgn(·) function represents the standard sign function, while the sat(·) function refers to the standard saturation function, which limits the output within the range [−1,1]. discontinuous switching of the control input as the system state approaches the sliding surface. This high-frequency oscillation can lead to actuator wear, system instability, and degraded control performance. In precision applications like shake tables, where accurate tracking of displacement, velocity, and acceleration is critical, chattering can significantly reduce control accuracy and system lifespan.

To address this problem, a fuzzy inference mechanism was incorporated into the sliding mode control design, resulting in FSMC. FSMC mitigates chattering by dynamically adjusting the boundary layer thickness through fuzzy logic. In traditional SMC, discontinuous control actions produce high-frequency oscillations that adversely affect performance. In contrast, the fuzzy system adaptively fine-tunes the boundary layer thickness based on real-time system states, such as velocity and acceleration errors.

TABLE 1 FUZZY RULES RELATED TO FUZZY SLIDING MODE CONTROLLER WITH SPEED AND ACCELERATION ERRORS

		Acceleration Error				
		nb	nm	Ze	pe	pb
Velocity Error	nb	nb	nb	Nm	nm	ze
	nm	nb	nm	Nm	ze	pm
	ze	nm	nm	Ze	pm	pm
	pm	nm	ze	Pm	pm	pb
	pb	ze	pm	Pm	pb	pb

This adaptive adjustment ensures a smoother transition between control states, minimizing abrupt changes in the control signal. Fuzzy rules dynamically modify the saturation function within the control law, preserving robust performance while effectively reducing chattering. Consequently, FSMC enhances both control precision and system stability, even under varying conditions and external disturbances, as validated through experimental results.

TABLE 2 THE VALUES OF THE DESIGNED CONTROLLER

Parameter	Value
β_{min}	18
β_{max}	22
$\hat{\beta}$	19.9
J_{min}	0.000577 kgm^2
J_{max}	0.001421 kgm^2
$\hat{J}$	.00090596 kgm^2
k	0.88
φ	0.01

Table 1 presents the fuzzy controller's rule base, where each input variable is divided into five membership functions: negative big (nb), negative medium (nm), zero (ze), positive medium (pm), and positive big (pb). A schematic diagram of the proposed supervisory controller based on the fuzzy sliding mode methodology is shown in Fig.1.To ensure the reproducibility of our results, detailed information regarding the tuning of FSMC is provided. The membership functions were designed as triangular shapes with 50% overlap, and the fuzzy rule base was determined through expert knowledge and iterative optimization based on minimizing the root mean square error (RMSE) of the control output. The sliding surface parameters λ and η were initially selected based on system dynamics and then fine-tuned through grid search within predefined stability margins. The gains of the equivalent control law and switching control components were adjusted using trial-and-error guided by Lyapunov stability criteria. Table 2 summarizes all final parameter values used in the

experiments, providing a complete reference for replicating the controller design and validation process. Design of adaptive filters (AEKF and AUKF)

The integration of the MEMS accelerometer, encoder, and camera sensor is performed through a data fusion process, where each sensor contributes complementary information to estimate the shake table's displacement, velocity, and acceleration. To optimally combine these measurements, Extended Kalman Filter (EKF) and Unscented Kalman Filter (UKF) techniques are employed.

The Kalman filter is a recursive algorithm that estimates the state of a dynamic system by processing noisy measurements in real-time, without the need to store previous data. It achieves this by fusing model-based predictions with actual observations [31]. However, due to the high nonlinearity of the system analyzed in this study, the conventional Kalman filter is inadequate. Therefore, the EKF and UKF are adopted to address the nonlinearities. The UKF, leveraging the unscented transformation, directly propagates the mean and covariance through nonlinear dynamics, offering a more accurate state estimation compared to linearization-based approaches. Although slightly more computationally demanding than the EKF, the UKF's enhanced capability in handling nonlinear systems makes it particularly suitable for high-precision applications such as seismic tracking in shake tables.

Remark 3: Compared to the linearization-based EKF, the UKF improves estimation accuracy in highly nonlinear systems by eliminating the need for Jacobians and instead applying the unscented transformation on sigma points.

Adaptive filtering techniques dynamically adjust the process and measurement noise covariance matrices, Q and R, which are critical to filter performance. This study focuses on the adaptive estimation of these covariances. Two primary objectives are pursued: (1) implementing AEKF and AUKF algorithms to accurately estimate the table's state variables, and (2) analyzing and comparing the performance of AEKF and AUKF to highlight their respective strengths and limitations.

Since the shake table dynamics are modeled in continuous time, while the adaptive filters are formulated in discrete time, the fourth-order Runge-Kutta method is employed to discretize the system. This method numerically approximates the solutions of the ordinary differential equations governing the shake table, enabling the application of the discrete-time filtering algorithms.

$$y_k = \begin{bmatrix} y_{Encoder} + r_{Encoder} \\ y_{camera} + r_{camera} \\ y_{Acceleration} + r_{Acceleration} \end{bmatrix} \tag{21}$$

where $\left(r_{Encoder}, r_{camera}, r_{Acceleration}\right)$ are measurement noises. The measurement and process noise covariance terms are uncorrelated, possessing white noise characteristics and following a Gaussian distribution with a mean of zero. These noise terms have known covariance matrices R and Q, respectively.

How to measure displacement using image processing technique is explained. The purpose of image processing in this research is to measure the displacement response of the moving plate of the shaking table. For this purpose, a screen with a white background, in the middle of which a rectangular sign in black colour with specific dimensions is installed on the table as the desired target for tracking. A 30-frame camera is also placed at a certain distance from the target screen. The image matrix is formed by the following relation:

$$I(x,y) = I(x+u, y+v) \tag{22}$$

where I is the image matrix, u and v are the pixel displacement descriptors. The image processing algorithm looks for pixels in each column that have values lower than the threshold value. The threshold value is the value that separates the black rectangle from the image background. Any column in which the number of pixels with a value less than the threshold is close to the number of pixels of the width of the black rectangle is averaged from the spatial coordinates of those pixels, and vertical calculations end in that column. The number obtained from this average is the coordinate of the center of the black mark in the vertical direction. The same method is used to obtain the horizontal center of the mark. Hence, by procuring the precise coordinates of the mark's center within each frame, one can ascertain the displacement of the table. Equation (23) shows this process.

$$y = \frac{\sum i \in [0,R]^{i[I(i,yn) < T]}}{\sum i \in [0,R]^{1[I(i,yn) < T]}} \tag{23}$$

Where y is the coordinate of the center of the target in the vertical direction. R is the number of pixels in a column and T is the threshold value and yn is the columns to be processed and is obtained from equation (24). The center of the target in the horizontal direction is obtained in the same way.

$$yn = \sum_{j=1}^{n} \frac{c \times j}{n} \tag{24}$$

Here, according to the dimensions of the image and the black rectangle, the image is divided into 8 parts. In equation (24), n is equal to 8. C is the number of pixels in a row or the same number of columns. By having the coordinates of the center of the mark in each frame of the image, the displacement of the table is obtained in terms of the number of pixels, but the goal is to calculate the displacement of the meter in millimeters. Therefore, the dimensions of each pixel should be obtained in millimeters. For this, first, according to the dimensions of the black mark and the number of pixels it occupies in the image, the dimensions of each pixel can be

obtained in millimeters. A simple camera is used in this research. In summary, the discrete nonlinear system is as:

$$\begin{aligned} x_k &= f(x_{k-1}) + u_{k-1} + w_{k-1} \\ y_k &= h(x_k) + v_k \end{aligned} \tag{25}$$

Is the process noise, the function f represents a dynamic model, which may be nonlinear. Similarly, the function h represents a measurement model, which may also be nonlinear[31]. Furthermore, the covariance of process noise $Q_k = E\left[w_k w_k^T\right]$ is as:

$$Q_k = diag\left[q_k^1 \quad q_k^2 \quad q_k^3 \quad q_k^4 \quad q_k^5\right],\ q_k^n \rangle 0 \tag{26}$$

Ultimately, the $v_k \sim N(0, R_k)$ represents a measurement noise characterized by a Gaussian distribution with a mean of zero. This noise is referred to as white noise due to its constant power across all frequencies. The covariance of this noise, denoted by $R_k = E\left[v_k v_k^T\right]$, can be represented in the following mathematical expression.

$$R_k = diag\left[r_k^1 \quad r_k^2 \quad r_k^3\right] \quad r_k^m \rangle 0, \quad m = 1,2,3 \tag{27}$$

3-2-1-Estimation of Table Parameters using EKF

The Extended Kalman filter algorithm has two steps of prediction and updating as below [32].

• Prediction

$$\hat{x}_{k|k-1} = F_k \hat{x}_{k-1} + u_{k-1} \tag{28}$$

$$P_{k|k-1} = F_k P_{k-1} F_k^T + Q_{k-1} \tag{29}$$

• Update

$$S_{k|k-1} = H_k P_{k|k-1} H_k^T + R_k \tag{30}$$

$$K_k = F_k P_{k|k-1} H_k \left(S_{k|k-1}\right)^{-1} \tag{31}$$

$$\hat{Z}_{k|k-1} = h\left(\hat{x}_{k|k-1}\right) \tag{32}$$

$$\hat{x}_k = \hat{x}_{k|k-1} + K_k \left(y_k - \hat{y}_{k|k-1}\right) \tag{33}$$

$$P_{k-1} = (I - K_k H_k) P_{k|k-1} \tag{34}$$

$$F_k = \frac{\partial f}{\partial x}\Big|_{x=\hat{x}_{k-1}} \tag{35}$$

$$H_k = \frac{\partial h}{\partial x}\Big|_{x=\hat{x}_{k-1}} \tag{36}$$

Estimation of Table Parameters using UKF

The EKF is widely utilized for estimating the states of nonlinear continuous-time systems by combining model-based predictions with real-time measurements. However, EKF requires linearization of the nonlinear system dynamics around the current estimated state at each time step. In complex systems such as the PMSM, this linearization process must be repeated continuously and can result in substantial computational complexity. Furthermore, the resulting linearized equations may become increasingly intricate, thereby adding to the processing burden.

In contrast, the UKF serves as a highly effective alternative to the EKF. Rather than linearizing the differential equations, the UKF utilizes the unscented transformation (UT) to directly propagate the mean and covariance of the state distribution through the nonlinear functions [33]. The UT provides a more accurate representation of the nonlinear transformations by capturing higher-order moments, which leads to improved estimation performance, especially in systems characterized by significant nonlinearities and model uncertainties.

This advantage is clearly reflected in the shake table experiments conducted in this study, where the UKF demonstrated superior accuracy and robustness compared to the EKF. The estimation process using UKF is described as follows:

• Initialization:

$$\begin{aligned} \hat{x}_0 &= E(x_0) \\ P_0 &= E((x_0 - \hat{x}_0)(x_0 - \hat{x}_0)^T) \\ W_0^m &= \frac{\lambda}{L+\lambda} \\ W_0^c &= \frac{\lambda}{L+\lambda} + (n - \alpha^2 + \beta) \\ W_i^m &= W_i^c = \frac{1}{2(\lambda + L)}\ ,\ i = 1, \ldots, 2L \\ \lambda &= \alpha^2 (L + \kappa) - L \end{aligned} \tag{37}$$

where λ represents a scaling parameter, which is determined by the constant parameters $0 \le \alpha \le 1$ and κ [34]. L denotes the dimensions of the state vector. Additionally, β is a non-negative parameter . When dealing with a Gaussian prior, the optimal value for β is considered to be 2 [34].

• Sigma Points Calculation and Time Update:

A set of weighted sigma points x_{k-1} is generated by

$$\begin{aligned} &x_{k-1} = \\ &\left[\hat{x}_{k-1} \quad \hat{x}_{k-1} + \sqrt{L+\lambda}\left(\sqrt{P_{k-1}}\right)_i \quad \hat{x}_{k-1} - \sqrt{L+\lambda}\left(\sqrt{P_{k-1}}\right)_i\right] \\ &i = 1, \ldots, n \end{aligned} \tag{38}$$

Cholesky decomposition is used to calculate $\sqrt{P_{k-1}}$, and the subscript i represents the column of the matrix.

$$\begin{aligned} x_{i,k|k-1} &= f(x_{i,k-1}) \\ \hat{x}_{k|k-1} &= \sum_{i=0}^{2L} W_i^m x_{i,k|k-1} \\ P_{k|k-1} &= \sum_{i=0}^{2L} W_i^c (x_{i,k|k-1} - \hat{x}_{k|k-1})(x_{i,k|k-1} - \hat{x}_{k|k-1})^T + Q_k \\ y_{i,k|k-1} &= h(x_{i,k|k-1}) \\ \hat{y}_{k|k-1} &= \sum_{i=0}^{2L} W_i^m y_{i,k|k-1} \end{aligned} \tag{39}$$

• Measurement Update:

$$\begin{aligned} P_k^{\hat{y}\hat{y}} &= \sum_{i=0}^{2L} W_i^m [y_{i,k|k-1} - \hat{y}_{k|k-1}][y_{i,k|k-1} - \hat{y}_{k|k-1}]^T + R_k \\ P_k^{\hat{x}\hat{y}} &= \sum_{i=0}^{2L} W_i^c [x_{i,k|k-1} - \hat{x}_{k|k-1}][y_{i,k|k-1} - \hat{y}_{k|k-1}]^T \\ K_k &= P_k^{\hat{x}\hat{y}} P_k^{\hat{y}\hat{y}} \\ \hat{x}_k &= \hat{x}_{k|k-1} + K_k \left[y_k - \hat{y}_{k|k-1}\right] \\ P_k &= P_{k|k-1} - K_k P_k^{\hat{y}\hat{y}} K_k^T \end{aligned} \tag{40}$$

During the forecasting stage, the model information serves as a vital factor, whereas the measurement data is incorporated into the estimates in the data assimilation stage.

Innovative Adaptive Algorithm Utilizing the Steepest Descent Method

In adaptive filtering algorithms, the process and measurement noise covariance matrices, denoted as Q and R respectively, serve as critical parameters that directly influence the performance and robustness of the estimator [35], [36]. In traditional Kalman filtering frameworks, these matrices are typically assumed to be known a priori and remain fixed throughout the estimation process. However, in many real-world applications, particularly in dynamic and uncertain environments, the statistical properties of noise may evolve over time due to changing operational conditions, sensor degradation, or environmental disturbances. As a consequence, maintaining static covariance assumptions can severely impair filter performance, leading to biased estimates and loss of optimality. To overcome these limitations, this study introduces a recursive covariance adaptation mechanism based on the steepest descent method. The steepest descent technique is a classical yet powerful optimization approach widely employed in adaptive filtering, offering an efficient means of iteratively minimizing cost functions associated with estimation errors. By leveraging the steepest descent principle, the proposed adaptation algorithm updates Q and R in real time, thereby enabling the filter to remain responsive to nonstationary noise characteristics.

The core idea behind the proposed adaptation strategy is to minimize the discrepancy between the empirical innovation covariance, derived from actual measurement residuals, and the theoretical innovation covariance predicted by the Kalman filter. Specifically, a cost function is formulated based on the norm of the difference between these two covariance matrices. The steepest descent method is then applied to adjust Q and R iteratively in the direction that reduces this cost, thereby ensuring that the filter maintains consistency and optimality even under time-varying noise conditions. This dynamic adjustment mechanism not only enhances the adaptability of the Kalman filter but also improves its robustness against modeling inaccuracies and external perturbations, making it particularly suitable for practical applications where noise environments are unpredictable and rapidly changing. In order to accomplish this objective, the initial step involves defining the disparity between the measurements in the following manner:

$$e_k = y_k - \hat{y}_{k|k-1} \tag{41}$$

Here, Z_k and $\hat{Z}_{k|k-1}$ are the real measurement and its estimated value, respectively. The remaining actual covariance of the above relationship is estimated by averaging this sequence according to the following relationship.

$$\hat{C}_{ek} = \frac{1}{M} \sum_{j=k-M+1}^{k} e_j e_j^T \tag{42}$$

The size of the estimation window is denoted by M. Deterministic and stochastic methods are employed to select the optimal size of the moving window. In the realm of deterministic techniques, an optimization problem is typically characterized by the deliberate selection of a suitable objective function, while taking into account the constraints imposed by limited memory[37]. Now, having the actual covariance $\hat{C}_{ek}$ and the theoretical covariance $S_{k|k-1}$ of the system, the cost function is defined as follows [38]:

$$J_k = \frac{1}{2} tr\left\{\left(S_{k|k-1} - \hat{C}_{ek}\right)\left(S_{k|k-1} - \hat{C}_{ek}\right)^T\right\} \tag{43}$$

The objective of employing sequence-based strategies for innovation is to minimize $S_{k|k-1} - \hat{C}_{ek}$ by altering R and Q. Hence, to minimize the cost function, it is crucial to ensure that the actual and theoretical covariance are identical. If there is a difference between the process and measurement noise covariance's from their actual values, it leads to a difference between these two covariance. The adaptive algorithm for process and measurement noise covariances is as follows:

$$q_k^n = \left|\lambda_{q,k}^n q_{k-1}^n + \mu_{q,k}^n\right| \qquad n = 1,2,3,4,5 \tag{44}$$

$$r_{k+1}^m = \left|\lambda_{r,k+1}^m r_k^m + \mu_{r,k+1}^m\right| \qquad m = 1,2,3 \tag{45}$$

Where q_k^n and r_{k+1}^m, representing the Q_k and R_k matrices respectively. The primary objective is to refine the values of $\lambda_{r,k+1}^m$, $\mu_{r,k+1}^m$, $\lambda_{q,k}^n$ and $\mu_{q,k}^n$ using the steepest descent technique. This technique aims to minimize the value of J_k as much as possible.

$$\lambda_{r,k+1}^m = \lambda_{r,k}^m - \eta_k^R \frac{\partial J_k}{\partial \lambda_{r,k}^m} = \lambda_{r,k}^m - \eta_k^R \frac{\partial J_k}{\partial r_k^m}\frac{\partial r_k^m}{\partial \lambda_{r,k}^m} \tag{46}$$

$$\mu_{r,k+1}^m = \mu_{r,k}^m - \eta_k^R \frac{\partial J_k}{\partial \mu_{r,k}^m} = \mu_{r,k}^m - \eta_k^R \frac{\partial J_k}{\partial r_k^m}\frac{\partial r_k^m}{\partial \mu_{r,k}^m} \tag{47}$$

$$\lambda_{q,k}^n = \lambda_{q,k-1}^n - \eta_k^Q \frac{\partial J_k}{\partial \lambda_{q,k-1}^n} = \lambda_{q,k-1}^n - \eta_k^R \frac{\partial J_k}{\partial q_{k-1}^m}\frac{\partial q_{k-1}^m}{\partial \lambda_{q,k-1}^n} \tag{48}$$

$$\mu_{q,k}^n = \mu_{q,k-1}^n - \eta_k^Q \frac{\partial J_k}{\partial q_{q,k-1}^n} = \mu_{q,k-1}^n - \eta_k^Q \frac{\partial J_k}{\partial q_{k-1}^n}\frac{\partial q_{k-1}^n}{\partial q_{q,k-1}^n} \tag{49}$$

The training parameters η_k^R and η_k^Q are selected based on empirical evidence. For relations (46), (47), (48) and (49), the following equalities hold:

$$\frac{\partial r_k^m}{\partial \lambda_{r,k}^m} = r_{k-1}^m.\mathrm{sgn}\left(\lambda_{r,k}^m r_{k-1}^m + \mu_{r,k}^m\right) \tag{50}$$

$$\frac{\partial r_k^m}{\partial \mu_{r,k}^m} = \mathrm{sgn}\left(\lambda_{r,k}^m r_{k-1}^m + \mu_{r,k}^m\right) \tag{51}$$

$$\frac{\partial q_{k-1}^m}{\partial \lambda_{q,k-1}^n} = q_{k-2}^n.\mathrm{sgn}\left(\lambda_{q,k-1}^n q_{k-2}^n + \mu_{q,k-1}^n\right) \tag{52}$$

$$\frac{\partial q_{k-1}^n}{\partial q_{q,k-1}^n} = \mathrm{sgn}\left(\lambda_{q,k-1}^n q_{k-2}^n + \mu_{q,k-1}^n\right) \tag{53}$$

The provided equations employ the notation sgn to represent the sign function. Furthermore, to calculate $\frac{\partial J_k}{\partial r_k^m}$ and $\frac{\partial J_k}{\partial q_{k-1}^m}$, the following relationship is used.

$$\frac{\partial J_k}{\partial r_k^m} = \frac{1}{2} tr\left(\frac{\partial (S_{k|k-1} - \hat{C}_{ek})^2}{\partial r_k^m}\right) = tr\left(\left(\frac{\partial S_{k|k-1}}{\partial r_k^m} - \frac{\partial \hat{C}_{ek}}{\partial r_k^m}\right)(S_{k|k-1} - \hat{C}_{ek})\right) \tag{54}$$

By utilizing Equations (28) and (40), we can derive the following result.

$$\frac{\partial \hat{C}_{ek}}{\partial r_k^m} = 0 \tag{55}$$

$$\frac{\partial S_{k|k-1}}{\partial r_k^m} = \frac{\partial R_k}{\partial r_k^m} \tag{56}$$

Where $\frac{\partial R_k}{\partial r_k^m}$ is a square matrix with dimension m. Similarly, $\frac{\partial J_k}{\partial q_{k-1}^n}$ for q_{k-1}^n is expressed as

$$\frac{\partial J_k}{\partial q_{k-1}^n} = \frac{1}{2} tr\left(\frac{\partial (S_{k|k-1} - \hat{C}_{ek})^2}{\partial q_{k-1}^n}\right) = tr\left(\left(\frac{\partial S_{k|k-1}}{\partial q_{k-1}^n} - \frac{\partial \hat{C}_{ek}}{\partial q_{k-1}^n}\right)(S_{k|k-1} - \hat{C}_{ek})\right) \tag{57}$$

$$\frac{\partial \hat{C}_{ek}}{\partial q_{k-1}^n} = 0 \tag{58}$$

$$\frac{\partial S_{k|k-1}}{\partial q_{k-1}^n} = H_k \frac{\partial Q_k}{\partial q_{k-1}^n} H_k^T \tag{59}$$

Where $\frac{\partial Q_k}{\partial q_{k-1}^n}$ is a square matrix with dimension n. Finally, we can express the laws for adapting coefficients as follows:

$$\lambda_{r,k+1}^m = \lambda_{r,k}^m - \eta_k^R.r_{k-1}^m.\mathrm{sgn}\left(\lambda_{r,k\ k-1}^m r^m + \mu_{r,k}^m\right) tr\left(\left(\frac{\partial R_k}{\partial r_k^m}\right)\left(S_{k|k-1} - \hat{C}_{ek}\right)\right) \tag{60}$$

$$\mu_{r,k+1}^m = \mu_{r,k}^m - \eta_k^R.\mathrm{sgn}\left(\lambda_{r,k\ k-1}^m r^m + \mu_{r,k}^m\right) tr\left(\left(\frac{\partial R_k}{\partial r_k^m}\right)\left(S_{k|k-1} - \hat{C}_{ek}\right)\right) \tag{61}$$

$$\lambda_{q,k}^n = \lambda_{q,k-1}^n - \eta_k^Q.q_{k-2}^n.\mathrm{sgn}\left(\lambda_{q,k-1}^n q_{k-2}^n + \mu_{q,k-1}^n\right) tr\left(\left(H_k \frac{\partial Q_{k-1}}{\partial q_{k-1}^n} H_k^T\right)\left(S_{k|k-1} - \hat{C}_{ek}\right)\right) \tag{62}$$

$$\mu_{q,k}^n = \mu_{q,k-1}^n - \eta_k^Q.\mathrm{sgn}\left(\lambda_{q,k-1}^n q_{k-2}^n + \mu_{q,k-1}^n\right) tr\left(\left(H_k \frac{\partial Q_{k-1}}{\partial q_{k-1}^n} H_k^T\right)\left(S_{k|k-1} - \hat{C}_{ek}\right)\right) \tag{63}$$

TABLE 3 PARAMETERS OF THE BALL-SCREW-DRIVEN SERVOMECHANISM

Parameter	Value	Units
L_d	0.00525	H
L_q	0.00525	H
R	0.9585	Ohm
p	8	_
β	0.0003035	Nm/rad/s
λ	0.1827	v/rad/s
η	%90	_
j	0.00805512	Kgm^2
h	20	Mm
m	16.75	Kg
m_1	10	Kg

Figure 2 illustrates the block diagram of the proposed adaptive filter. As shown, measurements from three linear encoders, a camera, and an accelerometer are fed into the AEKF/AUKF to estimate all relevant system states. The estimated linear velocity is processed by the feedback filter, which subtracts it from the reference input representing the desired earthquake ground motion. The resulting velocity error is then passed to the FSMC to generate appropriate control signals. The proposed method, combining FSMC with AEKF/AUKF for shake table control, significantly enhances the accuracy and robustness of seismic simulations. Its ability to handle system nonlinearities, sensor noise, and payload variations improves the reliability of shake table tests, thereby contributing to the development of safer and more resilient structures.

III. Results of Experimental Setup Testing

To evaluate the proposed control strategy for regulating displacement, velocity, and acceleration, an experimental study was conducted at Arak University [26] using a uniaxial earthquake simulator, as shown in Fig. 2. The shake table is driven by a PMSM coupled to a ball-screw mechanism, capable of achieving a maximum velocity of 100 mm/s and an acceleration of 2g, suitable for replicating moderate seismic events. The control system includes a servo drive, a Windows-based host PC, an ATMega32 microcontroller, an Advantech PCI-1716 DAQ card, a SCXI-1000 signal conditioner, and analog input modules. A linear encoder with 5 μm resolution measures the stage displacement, while a shaft encoder operating at 2500 pulses per revolution monitors the motor shaft angle. An ADXL203 analog accelerometer captures horizontal acceleration, and a camera operating at 30 fps provides additional displacement measurements. The sampling period for model discretization and controller implementation is set to 1 ms. Sensor data from the linear encoder are transmitted to the microcontroller for real-time processing. The parameters of the ball-screw-driven servomechanism are summarized in Table 3.

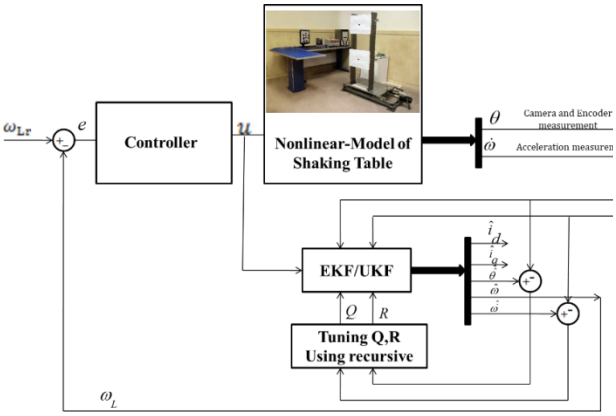

Fig.2.The uniaxial earthquake simulator at Arak University

The microcontroller calculates the position of the shake table and sends it to the DAQ card as a 16-bit word. The camera also sends data to the computer via the USB port. Acceleration data are also acquired by the DAQ card connected to the PC where the control program is implemented in MATLAB software. Furthermore, for safety reasons two infrared CNY70 limit switches are used to shut down the system in case the stage travel exceeds the predefined ±90-mm stroke range.

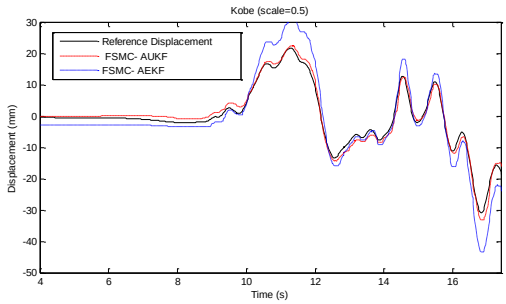

(A)

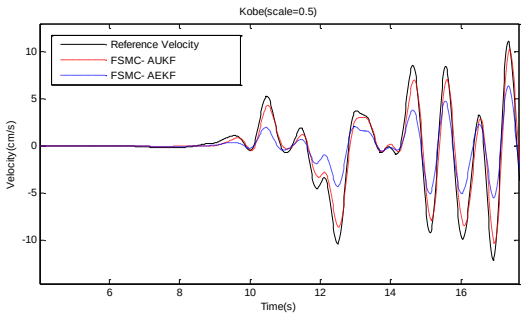

(B)

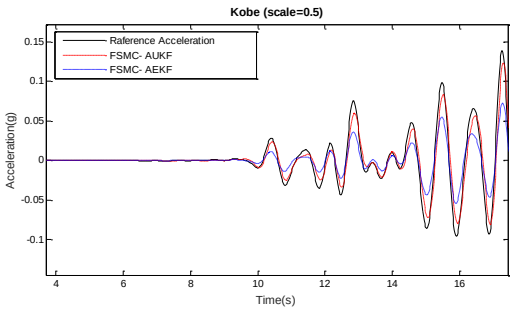

(C)

Fig.3. A Comparison between Reference Displacement (A), Velocity (B) and Acceleration (C) for Kobe Earthquake and Laboratory Test Results without structure installed on the shake table

As calibration is a critical step in ensuring the accuracy and reliability of the measurement system. The linear encoder, MEMS accelerometer, and camera system is all calibrated prior to the experiments. The linear encoder was calibrated by comparing its displacement measurements to a high-precision micrometer. The MEMS accelerometer was calibrated using a vibration table with known acceleration profiles. For the camera system, calibration involved determining the pixel-to-millimeter conversion factor by measuring a target of known dimensions at various distances. This process was crucial for minimizing measurement errors and ensuring the data fusion algorithms provided accurate state estimates, enhancing the overall methodology. Environmental disturbances such as EMI, vibrations, temperature variations, and dust significantly affect the performance of measurement sensors within control systems. While these challenges cannot be entirely eliminated, the integration of noise filtering, sensor shielding, and multi-sensor fusion techniques effectively mitigates their impact. This study highlights the importance of designing resilient control systems to address these issues, ensuring reliable operation and high precision in dynamic testing environments. The proposed control framework has been successfully implemented on the shake table using MATLAB. For evaluation, scaled versions of two significant seismic events—namely the Kobe and Chalfant earthquakes—were employed as reference inputs for displacement tracking and dynamic response analysis.

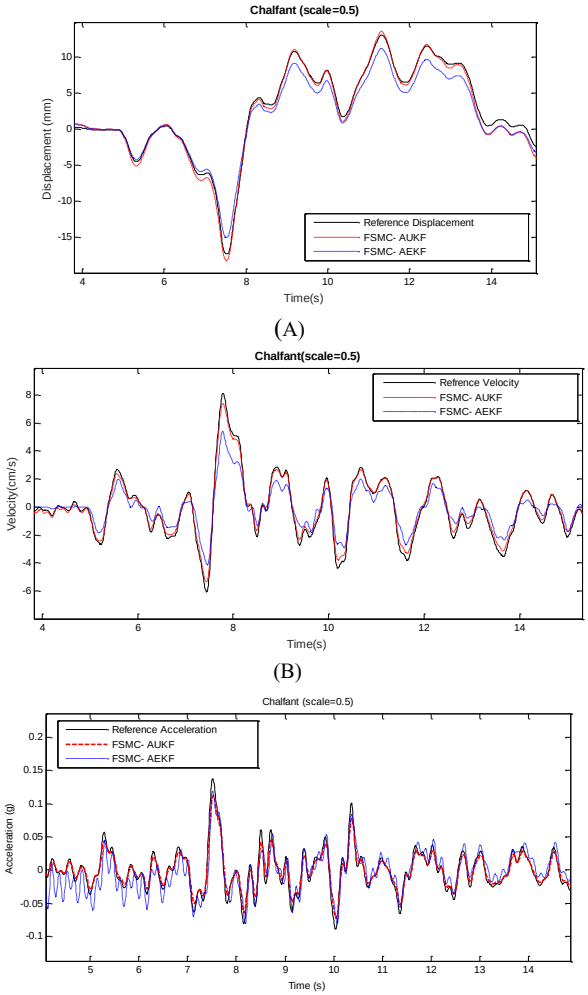

Fig .4. A Comparison between Reference Displacement (A), Velocity (B) and Acceleration (C) for Chalfant Earthquake and Laboratory Test Results without structure installed on the shake table

Figures 3(A)–(C) present a comparative assessment of tracking performance for different controller configurations, particularly the supervisory control scheme that integrates AEKF/AUKF-based sensor fusion with FSMC. As shown in Figure 3(A), the control system incorporating AEKF fails to track the displacement trajectory with sufficient precision. In contrast, the control system based on AUKF in conjunction with FSMC achieves a significant reduction in displacement tracking error. Similar performance enhancements are evident in velocity and acceleration tracking, as depicted in Figures 3(B) and 3(C), respectively. These outcomes highlight the superior estimation and control capabilities of the proposed AUKF-based FSMC framework, demonstrating its effectiveness in accurately reproducing complex earthquake motion profiles. When executing the adaptive algorithm, the initial values for the parameters $\lambda_{r,1}$, $\mu_{r,1}$, $\lambda_{q,0}$, and $\mu_{q,0}$ are established. These parameters should not be chosen too small, because of the effect of these parameters on R and Q. At the beginning of the process, R should not be smaller than its real value and Q should not be bigger than its real value. Based on the effect that η_k^R and η_k^Q have on R and Q respectively, η_k^R is chosen around 0.1 and η_k^Q can be chosen larger or smaller than this value.

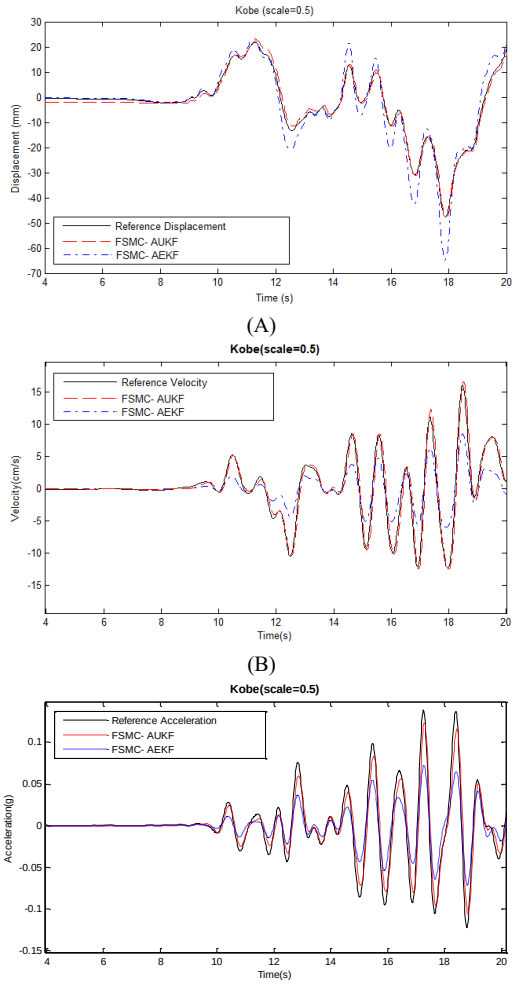

Fig.5. (A) Comparison between Reference Displacement, Velocity (B) and Acceleration (C) for Kobe Earthquake and Laboratory Test Results with structure installed on the shake table

Figures 4 (A)–(C) illustrate the trajectory tracking performance of the proposed control framework during the Chalfant earthquake scenario. The evaluation focuses on displacement, velocity, and acceleration responses over a representative short time window. Experimental results were obtained using real seismic data to assess the method's effectiveness in capturing acceleration dynamics. The figures compare the system's response under AUKF- and AEKF-based control strategies against the reference Chalfant earthquake records. In all three cases, the AUKF-based approach consistently outperforms its AEKF counterpart, achieving more accurate tracking of the target trajectories. These comprehensive experimental findings reinforce the effectiveness of integrating AUKF with FSMC,

confirming its superior capability in accurately tracking displacement, velocity, and acceleration under realistic earthquake conditions.

According to the findings provided, the incorporation of the FSMC and the AUKF-based technique on the shake table yielded a notable decrease in errors related to the tracking of displacement, velocity, and acceleration. To evaluate the resilience of the proposed controller, supplementary shake table experiments were performed using a mounted structure weighing 11.9 kilograms. Figure 2 depicts the shake table along with the structure securely mounted on its surface.

Tables 4 and 5 provide the root mean square error (RMSE) values. These results pertain to designs utilizing both AUKF and AEKF in conjunction with FSMC strategy, analyzed within the time domain. The tracking errors presented as follows:

$$Err_{RMS} = \left[\frac{1}{N}\sum_{i=0}^{N}\left(x[i]-x_{ref}[i]\right)^2\right]^{\frac{1}{2}}$$

The variable x_{ref} is utilized to represent the signal of interest that is to be tracked, which may include parameters such as displacement, velocity, or acceleration. Additionally, we generate a simulated signal that corresponds to the reference signal. The variable N indicates the quantity of data points measured in each experiment.

TABLE 4 RMSE WITHOUT STRUCTURE INSTALLED ON THE SHAKE TABLE FOR THE KOBE AND CHALFANT SAMPLE EARTHQUAKE

Earthquake	Controller and Estimator	Tracking Error		
		Displacement	Velocity	Acceleration
Kobe	PID	9.12	1.122	1.235
	FSMC+EKF	0.598	0.831	0.932
	FSMC+UKF	0.471	0.567	0.673
	FSMC+AEKF	0.417	0.499	0.892
	FSMC+AUKF	0.294	0.311	0.434
Chalfant	PID	9.198	1.108	1.198
	FSMC+EKF	0.489	0.606	0.787
	FSMC+UKF	0.301	0501	0.690
	FSMC+AEKF	0.312	0.475	0.553
	FSMC+AUKF	0.0923	0.399	0.484

Figures 5(A)–(C) display the system's performance in tracking displacement, velocity, and acceleration under conditions involving parametric uncertainty. The combination of FSMC and the AUKF-based estimation approach exhibited a strong degree of robustness, successfully tracking the reference trajectories across all dynamic variables.

TABLE 5 RMSE WITH THE STRUCTURE INSTALLED ON THE SHAKE TABLE FOR THE KOBE AND CHALFANT SAMPLE EARTHQUAKE

Earthquake	Controller and Estimator	Tracking Error		
		Displacement	Velocity	Acceleration
Kobe	PID	9.122	1.245	1.465
	FSMC+EKF	0.632	0.912	1.003
	FSMC+UKF	0.512	0.611	0.765
	FSMC+AEKF	0.499	0.832	0962
	FSMC+AUKF	0.386	0.457	0.603
Chalfant	PID	9.987	1.199	1.532
	FSMC+EKF	0.622	0.901	0.991
	FSMC+UKF	0.403	0.609	0.821
	FSMC+AEKF	0.5199	0.8013	0.9154
	FSMC+AUKF	0.296	0.5142	0.7021

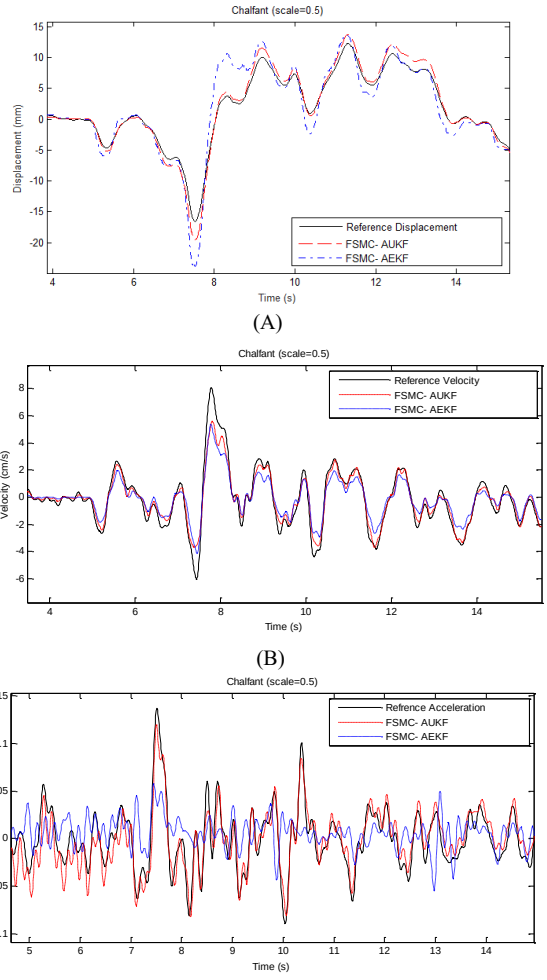

Fig.6. (A) Comparison between Reference Displacement, Velocity (B) and Acceleration (C) for Chalfant Earthquake and Laboratory Test Results with structure

In contrast, the AEKF-based control strategy failed to maintain acceptable tracking accuracy, particularly in the presence of model uncertainties. Further insights are provided in Figures 6(A)–(C), which compare the tracking performance of the supervisory controllers—specifically the integration of FSMC with either AEKF or AUKF—during the Chalfant earthquake scenario under uncertainty. The results clearly indicate that the FSMC+AUKF configuration achieves significantly lower errors across displacement, velocity, and acceleration trajectories. This underscores the advantage of the proposed adaptive filtering and control scheme in uncertain and nonlinear dynamic environments. The AUKF-based control consistently outperforms the AEKF-based control in trajectory tracking across all scenarios, as evidenced by the RMSE in the time domain. Extensive experimental results clearly demonstrate that

combining the AUKF and FSMC techniques with reference velocity records yields superior control performance for tracking displacement, velocity, and acceleration trajectories. In summary, the integration of AEKF/AUKF with FSMC significantly enhances the controller's adaptability, accuracy, and overall controllability, offering a robust control strategy well-suited for earthquake simulator applications. Furthermore, the experimental findings highlight the AUKF's notable superiority over the AEKF in trajectory tracking, achieving consistently lower RMSE values for displacement, velocity, and acceleration. Specifically, during the tracking of seismic profiles such as the Kobe and Chalfant earthquakes, the AUKF-based system demonstrated superior accuracy and stability, even under varying conditions and in the presence of parameter uncertainties.

TABLE 6 COMPARISON OF CONTROL INPUT CHATTERING

Control Method	RMS Voltage(V)	Relative Reduction
Standard SMS	12.45	20%
Proposed FSMC	4.08	67%

To rigorously validate the proposed FSMC-AUKF framework, its performance was compared against PID and FSMC-EKF/UKF based controllers under identical experimental conditions. As shown in Table 4 and 5, the proposed method reduced displacement, velocity, and acceleration RMSE by 45–60% compared to PID and 32–52% compared to FSMC-EKF/UKF. The adaptive noise covariance in AUKF outperformed conventional EKF/UKF by 18–28%, particularly under payload uncertainties. These results confirm that the synergy of fuzzy boundary layer adaptation and adaptive filtering uniquely addresses the limitations of existing methods in high-precision seismic tracking. Also, to quantify the chattering suppression, the RMS values of the control input voltage were computed for both the standard SMC and FSMC during the high-frequency phase of the Kobe earthquake simulation (10–15 seconds). As demonstrated in Table 6, the FSMC reduces the RMS voltage from 12.45 V (SMC) to 4.08 V, achieving a 67% reduction in chattering.

Table 7 presents a comparative analysis of the computational cost associated with the implemented algorithms (PID, FSMC+EKF, FSMC+UKF, FSMC-AEKF, and FSMC-AUKF). All methods were executed on identical hardware specifications (Intel Core i7-9700K CPU, 16 GB RAM) to ensure a fair comparison. Among the evaluated approaches, FSMC-AUKF exhibits a higher computational burden compared to the conventional PID controller, primarily due to the incorporation of adaptive filtering mechanisms and fuzzy inference systems. Nonetheless, this increased computational demand is justified by the significantly enhanced tracking performance offered by the FSMC-AUKF method.

TABLE 7 COMPARISONS OF COMPUTATIONAL COST

Controller and Estimator	Computational Cost
PID	0.12
FSMC+EKF	0.15
FSMC+UKF	0.17
FSMC+AEKF	0.165
FSMC+AUKF	0.19

IV. Conclusion

This paper presented the development and application of a novel supervisory controller combining FSMC with AEKF and AUKF techniques for precise motion control of a laboratory-scale shake table. A structure was employed to mitigate chattering in the sliding mode control input, thereby improving the operational lifespan of the electric motors. An adaptive recursive method for noise covariance estimation was proposed, offering low computational complexity while ensuring the non-negativity of covariance matrix elements. Optimal state estimation was achieved through sensor fusion, integrating encoder, accelerometer, and camera data using Kalman filtering techniques. This fusion effectively compensated for sensor faults, maintaining system performance even under partial sensor failure. The image processing approach also demonstrated strong performance at a low cost. Through the proposed methodology, accurate estimation of the table velocity, previously unmeasurable, was accomplished using AEKF and AUKF. Two experimental setups were designed: one integrating FSMC with AUKF, and the other with AEKF. Results demonstrated that the proposed controller successfully suppressed excessive vibrations caused by the system's inherent flexibility. Furthermore, AUKF consistently achieved higher estimation accuracy compared to AEKF, despite similar computational complexity. Experimental validation using the Chalfant and Kobe earthquake records confirmed the controller's robustness in both stability and performance. While the experimental results are promising, several limitations must be acknowledged. The experiments were conducted on a laboratory-scale shake table with specific configurations. Broader validation across diverse payloads, actuator types, and environmental conditions is necessary for generalization. Moreover, challenges such as latency, hardware constraints, and unmodeled dynamics, typical in industrial applications, were not fully addressed. Future work will focus on extending validation to large-scale shake tables, integrating deep learning-based adaptive control methods, and optimizing computational efficiency for real-time embedded system implementation. These efforts aim to bridge the gap between laboratory research and industrial application.

References

[1] S. Bianchi et al., "Shake-table tests of innovative drift sensitive nonstructural elements in a low-damage structural system," Earthquake Engineering & Structural Dynamics, vol. 50, no. 9, pp. 2398-2420, 2021, doi: https://doi.org/10.1002/eqe.3452.

[2] S. Chen, H. Zhuang, D. Quan, J. Yuan, K. Zhao, and B. Ruan, "Shaking table test on the seismic response of large-scale subway station in a loess site: A case study," Soil Dynamics and Earthquake Engineering, vol. 123, pp. 173-184, 2019.

[3] H. Yang, D. Cong, Z. Yang, and J. Han, "A Practical Adaptive Sinusoidal Vibration Control Strategy for Electro-Hydraulic Shake Table," Journal of Vibration Engineering & Technologies, vol. 11, pp. 1725–1739, 2023

[4] S. Pampanin et al., "Triaxial shake table testing of an integrated low-damage building system," Earthquake Engineering & Structural Dynamics, 2023.

[5] M. Flah, M. Ragab, M. Lazhari, and M. Nehdi, "Localization and classification of structural damage using deep learning single-channel signal-based measurement," Automation in Construction, vol. 139, p. 104271, 2022.

[6] M. Diaz, P.-É. Charbonnel, and L. Chamoin, "A new Kalman filter approach for structural parameter tracking: application to the monitoring of damaging structures tested on shaking-tables," Mechanical Systems and Signal Processing, vol. 182, p. 109529, 2023.

[7] M. A. Kuddus, J. Li, H. Hao, C. Li, and K. Bi, "Target-free vision-based technique for vibration measurements of structures subjected to out-of-plane movements," Engineering Structures, vol. 190, pp. 210-222, 2019.

[8] J. Wen, C. Zhao, and Z. Shi, "LSTM-based adaptive robust nonlinear controller design of a single-axis hydraulic shaking table," IET Control Theory & Applications, vol. 17, no. 7, pp. 825-836, 2023.

[9] A. Najafi and B. F. Spencer Jr, "Modified model-based control of shake tables for online acceleration tracking," Earthquake Engineering & Structural Dynamics, vol. 49, no. 15, pp. 1721-1737, 2020.

[10] J. Yao et al., "Sinusoidal acceleration harmonic estimation using the extended Kalman filter for an electro-hydraulic servo shaking table," Journal of Vibration and Control, vol. 21, no. 8, pp. 1566-1579, 2015.

[11] J. Yao, D. Di, G. Jiang, S. Gao, and H. Yan, "Real-time acceleration harmonics estimation for an electro-hydraulic servo shaking table using Kalman filter with a linear model," IEEE Transactions on Control Systems Technology, vol. 22, no. 2, pp. 794-800, 2013.

[12] Z. Lu, Z. Wang, Y. Zhou, and X. Lu, "Nonlinear dissipative devices in structural vibration control: A review," Journal of Sound and Vibration, vol. 423, pp. 18-49, 2018.

[13] J. Lu, H. Xie, L. Hu, H. Yang, and Y. Chen, "Variable-parameter feedforward control for centrifuge shaking table based on nonlinear frequency characteristic model," Mechanical Systems and Signal Processing, vol. 161, p. 108011, 2021.

[14] Y. Tang, G. Shen, Z.-C. Zhu, X. Li, and C.-F. Yang, "Time waveform replication for electro-hydraulic shaking table incorporating off-line iterative learning control and modified internal model control," Proceedings of the Institution of Mechanical Engineers, Part I: Journal of Systems and Control Engineering, vol. 228, no. 9, pp. 722-733, 2014, doi: 10.1177/0959651814536553.

[15] S. Welikala, H. Lin, and P. Antsaklis, "A Decentralized Analysis and Control Synthesis Approach for Networked Systems with Arbitrary Interconnections," arXiv preprint arXiv:2204.09756, 2022.

[16] F. Beltran-Carbajal and G. Silva-Navarro, "Output feedback dynamic control for trajectory tracking and vibration suppression," Applied Mathematical Modelling, vol. 79, pp. 793-808, 2020.

[17] G. Shen, G.-M. Lv, Z.-M. Ye, D.-C. Cong, and J.-W. Han, "Implementation of electrohydraulic shaking table controllers with a combined adaptive inverse control and minimal control synthesis algorithm," Iet control theory & applications, vol. 5, no. 13, pp. 1471-1483, 2011.

[18] T. B. Ma and F. Du, "Minimal control synthesis algorithm for panel vibration control," Advanced Materials Research, vol. 804, pp. 269-274, 2013.

[19] C.-h. Gao and X.-b. Yuan, "Development of the shaking table and array system technology in China," Advances in Civil Engineering, vol. 2019, 2019.

[20] O. A. Al-Fahdawi and L. R. Barroso, "Adaptive neuro-fuzzy and simple adaptive control methods for full three-dimensional coupled buildings subjected to bi-directional seismic excitations," Engineering Structures, vol. 232, p. 111798, 2021.

[21] A. S. Sayed, A. T. Azar, Z. F. Ibrahim, H. A. Ibrahim, N. A. Mohamed, and H. H. Ammar, "Deep learning based kinematic modeling of 3-rrr parallel manipulator," in Proceedings of the International Conference on Artificial Intelligence and Computer Vision (AICV2020), 2020: Springer, pp. 308-321.

[22] E. W. Suseno and A. Ma'arif, "Tuning of PID controller parameters with genetic algorithm method on DC motor," International Journal of Robotics and Control Systems, vol. 1, no. 1, pp. 41-53, 2021.

[23] H. Zhang, L. Wang, and W. Shi, "Seismic control of adaptive variable stiffness intelligent structures using fuzzy control strategy combined with LSTM," Journal of Building Engineering, vol. 78, p. 107549, 2023.

[24] K. Seki, M. Iwasaki, M. Kawafuku, H. Hirai, and K. Yasuda, "Adaptive compensation for reaction force with frequency variation in shaking table systems," IEEE Transactions on Industrial Electronics, vol. 56, no. 10, pp. 3864-3871, 2009.

[25] S. Strano and M. Terzo, "A non-linear robust control of a multi-purpose earthquake simulator," in Proceedings of the World Congress on Engineering, 2013, vol. 3.

[26] M. Soleymani, A. Khalatabari-S, and B. Ghanbari-S, "Fuzzy-sliding-mode supervisory control of a seismic shake table with variable payload for robust and precise acceleration tracking," Journal of earthquake Engineering, vol. 23, no. 4, pp. 539-556, 2019.

[27] M. Tárník and J. Murgaš, "Model reference adaptive control of permanent magnet synchronous motor," Journal of Electrical Engineering, vol. 62, no. 3, pp. 117-125, 2011.

[28] C. J. O'Rourke, M. M. Qasim, M. R. Overlin, and J. L. Kirtley, "A geometric interpretation of reference frames and transformations: dq0, clarke, and park," IEEE Transactions on Energy Conversion, vol. 34, no. 4, pp. 2070-2083, 2019.

[29] X. Li and G. Gong, "Objective-oriented genetic algorithm based dynamical sliding mode control for slurry level and air pressure in shield tunneling," Automation in Construction, vol. 109, p. 102987, 2020.

[30] H. Komurcugil, S. Biricik, S. Bayhan, and Z. Zhang, "Sliding mode control: Overview of its applications in

power converters," IEEE Industrial Electronics Magazine, vol. 15, no. 1, pp. 40-49, 2020.

[31] X. Cheng, X. Liu, X. Li, and Q. Yu, "An intelligent fusion estimation method for state of charge estimation of lithium-ion batteries," Energy, vol. 286, p. 129462, 2024.

[32] N. Kayhani, W. Zhao, B. McCabe, and A. P. Schoellig, "Tag-based visual-inertial localization of unmanned aerial vehicles in indoor construction environments using an on-manifold extended Kalman filter," Automation in Construction, vol. 135, p. 104112, 2022.

[33] H. Tang et al., "Feature extraction of multi-sensors for early bearing fault diagnosis using deep learning based on minimum unscented kalman filter," Engineering Applications of Artificial Intelligence, vol. 127, p. 107138, 2024.

[34] I. Ullah, Y. Shen, X. Su, C. Esposito, and C. Choi, "A localization based on unscented Kalman filter and particle filter localization algorithms," IEEE Access, vol. 8, pp. 2233-2246, 2019.

[35] Y. Zhang, M. Li, Y. Zhang, Z. Hu, Q. Sun, and B. Lu, "An enhanced adaptive unscented kalman filter for vehicle state estimation," IEEE Transactions on Instrumentation and Measurement, vol. 71, pp. 1-12, 2022.

[36] D. Lee, G. Vukovich, and R. Lee, "Robust unscented Kalman filter for nanosat attitude estimation," International Journal of Control, Automation and Systems, vol. 15, pp. 2161-2173, 2017.

[37] J. H. Yoon, D. Y. Kim, and V. Shin, "Window length selection in linear receding horizon filtering," in 2008 International Conference on Control, Automation and Systems, 2008: IEEE, pp. 2463-2467.

[38] R.Havangi,F.Karimi, "Improvement of The Battery State of Charge Estimation Using Recursive Least Square Based Adaptive Extended Kalman Filter "International Journal of Industrial Electronics, Control and Optimization ,vol.7,no.2,pp.141-151,2024.

Nima Rajabi Namini *received the M.S. degree in Electrical Engineering from Arak University, Arak, Iran, in 2015, the Ph.D. degree in Control Engineering from the University of Birjand, Birjand, Iran, in 2024. His research interests include Control, Nonlinear Dynamic Systems, Robust Control, State Estimation and Filtering, evolutionary filtering, Multi-Sensor Data Fusion.*

Ramazan Havangi *received his M.S. and Ph.D. degrees from the K.N. Toosi University of Technology, Tehran, Iran, in 2003 and 2012, respectively. He is currently an Associate Professor of control systems with the Department of Electrical and Computer Engineering, University of Birjand, Birjand, Iran. His main research interests are inertial navigation, integrated navigation, estimation and filtering, evolutionary filtering, simultaneous localization and mapping, fuzzy, neural network, and soft computing.Email: Havangi@Birjand.ac.ir*

Amir Hossein Abolmasoumi received the B.S. degree in Electrical Engineering from University of Tehran in 2004, the M. Sc. degree from Tarbiat Modares University in 2007 and his PhD in control engineering department, Tarbiat Modares University, Tehran, Iran. He is currently with the Electrical Engineering department of Arak University. His research interests include stochastic switching systems, delayed dynamical systems and congestion control in communication networks.